

Structure, vibrational spectroscopy, and photochemistry of 5-phenoxy-1-phenyltetrazole in argon and nitrogen cryomatrices

A. Borba, L.I.L. Cabral, R. Fausto, and M.L.S. Cristiano

Abstract: The molecular structure, infrared spectra, and photochemistry of 5-phenoxy-1-phenyltetrazole (5PPT) isolated in argon and N₂ cryogenic matrices were investigated by infrared spectroscopy and theoretical calculations (DFT(B3LYP)/6-311++G(d,p)). Calculations yield two dissimilar minima on the potential energy surface of the molecule, both being eightfold degenerate by symmetry and belonging to the C₁ symmetry point group. Extensive analysis of the potential energy landscape of the molecule was performed. Upon consideration of the zero-point vibrational correction to the energy, the calculations predict that the higher energy minimum shall relax barrierlessly to the lower energy form, leading to conclude that the compound exists in a single conformer in the gas phase. Accordingly, a single conformer was observed and fully characterized spectroscopically upon isolation of the monomer of the compound in argon and nitrogen cryomatrices. UV-laser irradiation ($\lambda = 250$ nm) of matrix-isolated 5PPT leads to photocleavage of the tetrazole ring, with release of N₂ and formation of the corresponding carbodiimide.

Key words: tetrazole, 5-aryloxytetrazole, molecular structure, infrared spectra, UV-induced N₂ photoelimination.

Résumé : La structure moléculaire, les spectres infrarouges et la photochimie de 5-phénoxy-1-phényltétrazole (5PPT) isolé dans des matrices cryogéniques de l'argon et de N₂ ont été étudiés par spectroscopie d'infrarouges et calculs théoriques (DFT(B3LYP)/6-311++G(d,p)). Les calculs donnent deux minima différents sur la surface d'énergie potentielle de la molécule, les deux étant de huit fois dégénérés par symétrie et appartenant au groupe de points de symétrie C₁. Une analyse approfondie du paysage d'énergie potentielle de la molécule a été effectuée. Après examen des corrections du point zéro de vibration à l'énergie, les calculs prédisent que le minimum d'énergie plus élevée doit détendre sans barrière à la forme d'énergie plus faible, ce qui permet de conclure que le composé existe comme un seul conformère dans la phase gazeuse. En effet, un seul conformère a été observé, et caractérisé entièrement par spectroscopie, après l'isolement du monomère du composé dans des cryomatrices de l'argon et d'azote. Irradiation de 5PPT isolé en cryomatrice de l'argon avec laser UV ($\lambda = 250$ nm) conduit à photoclavage de l'hétérocycle tétrazole avec sortie de N₂ et production de la carbodiimide correspondante.

Mots-clés : tétrazole, 5-aryloxytétrazole, structure moléculaire, spectres infrarouges, photoélimination de N₂.

Introduction

Tetrazole¹ and derivatives remain a topic of intense research. The wide interest in this class of compounds derives mainly from their relevant applications in major areas, such as in medicine,² agriculture,³ the automobile industry,⁴ imaging technology,⁵ and coordination chemistry⁶ and also as high-energy materials.⁷ In drug design, 5-substituted tetrazoles are often used as a metabolically stable bioisosteric replacement for the carboxylic acid moiety⁸ and 1,5-disubstituted tetrazoles act as a mimic for the *cis*-amide bond.⁹

Additionally, tetrazoles play a major role in synthesis. Due to the strong electron-withdrawing properties of the heterocycle, 5-chloro-1-phenyltetrazole¹⁰ (1) (Scheme 1) has been used as derivatising agent for alcohols. The resulting tetrazolyl ethers proved to be excellent intermediates for reductive cleavage of the C–O bond catalysed by transition metals in phenols^{11,12} and in allylic,¹³ benzylic,¹⁴ and naphthylic alcohols.¹⁵ Etherification weakens the C–O bond of the original alcohol so that hydrogenolysis occurs easily and selectively across the longer bond in the tetrazolyl

ether (3) (Scheme 1, bond *a*). On the other hand, in ether 3, bond *b* (Scheme 1) is comparatively strong due to delocalization of the unshared electron pair on oxygen towards the electron-withdrawing heterocycle. This methodology for hydrogenolysis makes use of hydrogen donors, thus avoiding the use of molecular hydrogen, and the catalyst is easily filtered off and may be reused. The leaving group leads to formation of water-soluble tetrazolone (5) (Scheme 1).¹⁶

The photochemistry of tetrazoles, in solution and isolated in cryogenic matrices, has been reviewed.^{17,18} Generally, irradiation of tetrazoles in the UV spectral region leads to cleavage of the tetrazole ring. The photofragmentation pattern and the structure and stability of the photoproducts obtained are determined by the chemical nature and conformational flexibility of the substituents. If the molecule exhibits tautomerism, tautomer-selective photochemistry may take place.^{19–21}

The structural features that render tetrazolyl ethers excellent substrates for transfer hydrogenolysis may also influence their photochemistry. Among 1,5-disubstituted tetrazoles, 5-aryloxy-1-phenyltetrazoles appear to be especially interesting, since the

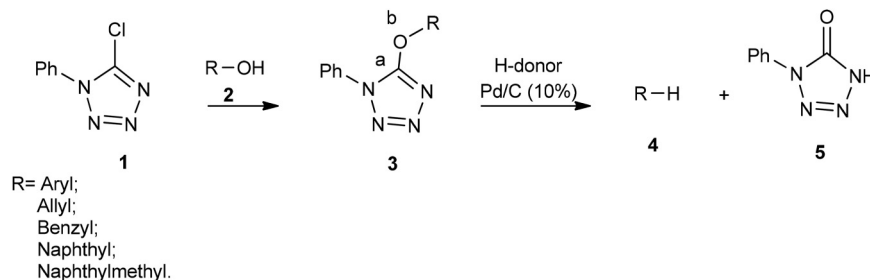
Received 12 January 2015. Accepted 7 April 2015.

A. Borba and R. Fausto. Department of Chemistry, University of Coimbra, P-3004-535 Coimbra, Portugal.

L.I.L. Cabral and M.L.S. Cristiano. CCMAR and Department of Chemistry and Pharmacy, F.C.T., University of Algarve, P-8005-039 Faro, Portugal.

Corresponding author: M.L.S. Cristiano (e-mail: mlscristiano@gmail.com).

This article is part of a Special Issue entitled "Advances and Applications in Physical Organic Chemistry" based on contributed papers from the 22nd International Conference on Physical Organic Chemistry (Ottawa, Canada, 2014).

Scheme 1. Tetrazolyl ethers **3** as intermediates for catalytic transfer hydrogenolysis of alcohols **2**.

central oxygen links an aromatic and an electron-withdrawing heteroaromatic system. Reported crystal structures for a representative library of aryloxy and naphthoxy tetrazoles²² reveal that, as expected, the central ether linkage (**3**) (**Scheme 1**) is much shorter on the tetrazolyl ether side (C–O *b* around 132 pm) than on the aryl or naphthyl side (O–C *a* around 143 pm), with C–O–C bond angles around 117°. As may be deduced from crystallographic analysis, in these heteroaromatic ethers the ether oxygen appears to show an approximate sp^2 hybridization²² and is strongly conjugated with the tetrazolyl ring system, but not with that of the phenyl or naphthyl substituent. The X-ray analyses also show that the plane of the naphthyl or aryl ring is nearly perpendicular to that of the tetrazolyl system.

Although the structure of aryloxy tetrazoles is well characterized in the condensed phase, there is no information regarding their structure for the isolated molecule situation. Furthermore, the photochemistry of 5-aryloxy tetrazoles has not been investigated. In this work, we discuss our recent findings on the monomeric structure and UV-induced photochemistry of 5-phenoxy-1-phenyl tetrazole (5PPT) (**3**) (**Scheme 1**; R = Ph), isolated in solid argon and N₂ cryomatrices. In this 1,5-disubstituted tetrazole, both substituents bear aromatic character and may, in principle, conjugate with the tetrazole ring. The interpretation of the experimental results was assisted by extensive DFT(B3LYP)/6-311++G(d,p) calculations on the structures of 5PPT and of putative photoproducts.

Experimental section

Chemicals and apparatus

All chemicals were used as purchased. Solvents for extraction were of technical grade. When required, solvents were freshly distilled from the appropriate drying agents before use. Analytical TLC was performed with silica gel 60 F254 plates. Melting points were recorded on a Stuart Scientific SMP3 melting point apparatus and are uncorrected. Mass spectra were obtained on a VG 7070E mass spectrometer by electron ionization at 70 eV. NMR (400 MHz) spectra were obtained on a Bruker AM-400 spectrometer using TMS as the internal reference (δ = 0.0 ppm). The ¹H NMR spectrum for 5PPT is provided as supporting information (Fig. S1) (see Supplementary material section).

Preparation of 5-phenoxy-1-phenyltetrazole (5PPT)

Phenol (630 mg, 6.65 mmol) was added to a suspension of NaH (520 mg, 2.16 mmol) in dry THF (20 mL) in anhydrous conditions. The mixture was stirred for 3 h at room temperature under N₂. Then, a solution of 5-chloro-1-phenyltetrazole **1** (1 g, 5.4 mmol) in dry THF (20 mL) was added and the final mixture was stirred overnight. Evaporation of the solvent followed by extraction with DCM (30 mL), washing of the organic layer with 2 mol L⁻¹ HCl (10 mL) and water (2 × 30 mL), and evaporation of combined organic extracts led to a solid. Recrystallization from ethanol–DCM (2:1) yielded the required crystalline product (1.06 g, 4.48 mmol, 83% yield), mp 116–118 °C. ¹H NMR (400 MHz, CDCl₃) δ : 7.24 (t, 1H, *J* = 7.1 Hz), 7.37 (td, 4H, *J* = 7.9 Hz, *J* = 15.9 Hz), 7.45 (d, 1H, *J* = 7.4 Hz), 7.51 (t, 2H, *J* = 7.6 Hz), 7.74 (d, 2H, *J* = 8.1 Hz).

Matrix preparation, infrared spectroscopy, and UV irradiation experiments

For preparing the low-temperature matrices, a solid sample of 5PPT was sublimated (at ~325 K) using a pyrex minioven placed in the vacuum chamber of the cryostat (APD Cryogenics close-cycle helium refrigeration system with a DE-202A expander). The vapor of the compound was deposited together with a large excess of inert gas (argon N60 or nitrogen N50, both obtained from Air Liquide) onto a cold (14–20 K) CsI substrate. The temperature was controlled and measured using a diode sensor connected to a Scientific Instruments digital temperature controller (model 9659) to within ±1 degree. In the matrix isolation annealing experiments, the temperature was varied in steps of 3° until ~25 K.

The IR spectra (4000–400 cm⁻¹) were collected with 0.5 cm⁻¹ spectral resolution using a Nicolet 6700 fourier transform infrared spectrometer equipped with a deuterated triglycine sulphate detector and a Ge/KBr beamsplitter. Modifications of the sample compartment of the spectrometer were made to accommodate the cryostat head and allow an efficient purging of the system by a continuous stream of dry air to avoid interference from atmospheric water and CO₂.

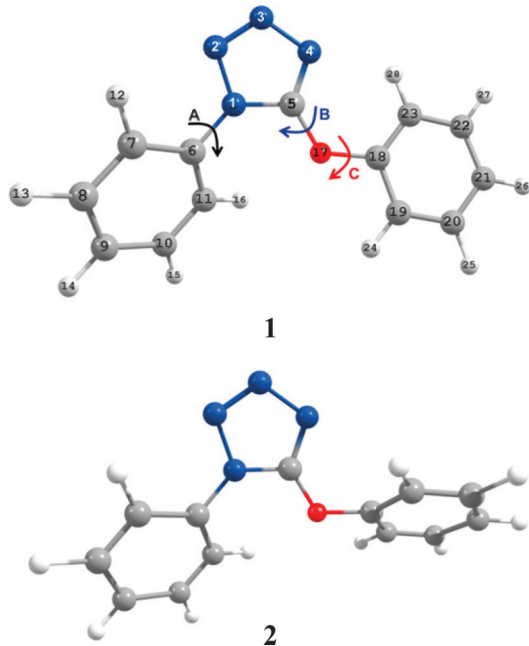
The UV irradiation (λ = 250 nm) of the matrices was carried out through the outer quartz window of the cryostat, with the frequency doubled signal beam of the Quanta-Ray MOPO-SL pulsed (10 ns) optical parametric oscillator (FWHM ~ 0.2 cm⁻¹, repetition rate 10 Hz, pulse energy ~1.0 mJ) pumped by a Nd:YAG laser.

Computational methods

The quantum chemical calculations were performed with the Gaussian 09 suite of programs²³ at the DFT(B3LYP)^{24–26} level of approximation using the 6-311++G(d,p) basis set.²⁷ Structures were optimized using the geometry direct inversion of the iterative subspace method,²⁸ with the nature of the obtained stationary points being checked by inspection of the corresponding Hessian matrix. Potential energy profiles for internal rotation were calculated by performing relaxed scans on the B3LYP/6-311++G(d,p) potential energy surface along the relevant coordinates. The transition state structures for conformational conversions were obtained using the synchronous transit-guided quasi-Newton method.²⁹

The B3LYP/6-311++G(d,p)-calculated vibrational frequencies were scaled by 0.978 and the resulting frequencies, together with the calculated intensities, were used to simulate the spectra shown in the figures. In these simulations, the absorptions were broadened by Lorentzian profiles (fwhm = 5 cm⁻¹) centered at the calculated (scaled) frequencies using the SYNSPEC software.³⁰ Note that the peak intensities in the simulated spectra (shown in units of “relative intensity”) differ from the calculated intensities (in km mol⁻¹) because they were set to satisfy the condition that the integrated band area in the simulated spectrum corresponds to the calculated infrared intensity. The theoretical normal modes were analyzed by carrying out the potential energy distribution calculations performed according to a procedure described in the literature.^{31,32} The set of internal coordinates used in the potential

Fig. 1. Structures of the 5PPT minimum energy forms and adopted atom numbering scheme. The three internal rotational degrees of freedom of the molecule are indicated by the arrows. The $C_{18}-O_{17}-C_5-N_1$ dihedral angle in forms **1** and **2** is approximately 178° and 169° , respectively. The geometries about the bonds A and C are discussed in detail in the text (see also Figs. 2 and 3).



energy distribution analysis was defined following the recommendations of Pulay et al.³³

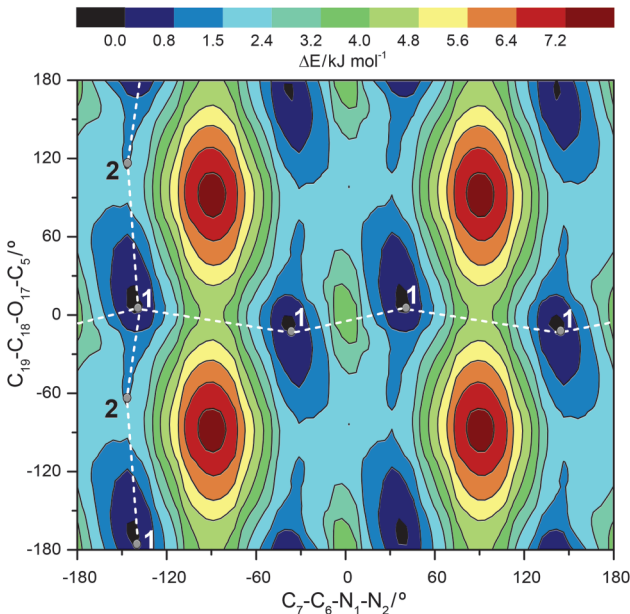
Results and discussion

Geometries and energies

The 5PPT molecule has three torsional degrees of freedom, corresponding to internal rotations around the C_6-N_1 (A in Fig. 1), $O_{17}-C_5$ (B), and $C_{18}-O_{17}$ (C) bonds (Fig. 1). All low-energy structures of the molecule were found to exhibit a conformation about the $O_{17}-C_5$ bond approximately *trans* (i.e., with the two phenyl groups of the molecule pointing to opposite directions). On the other hand, the alternative *cis* orientation brings the two phenyl groups in close spatial proximity, resulting in strong steric repulsions and considerably large energies. The conformational space of the molecule is then essentially determined by the arrangements around the C_6-N_1 (A) and $C_{18}-O_{17}$ (C) bonds, which are related with the orientation of each one of the phenyl groups relatively to the tetrazole ring.

The search on the B3LYP/6-311++G(d,p) potential energy surface of the molecule revealed the existence of two different minima, **1** and **2** (Fig. 1), both being eightfold degenerate by symmetry and belonging to the C_1 symmetry point group. According to the calculations, the energy difference between the two different minima amounts to 1.14 kJ mol^{-1} (zero-point corrected energy difference; 1.31 kJ mol^{-1} if counted from the bottom of the potential wells), with the lower energy minimum having a slightly larger dipole moment (5.30 versus 5.23 D in **2**). A potential energy map showing the location of the two forms as a function of the conformationally relevant C_6-N_1 and $C_{18}-O_{17}$ torsional coordinates is shown in Fig. 2. Figure 3 shows the relaxed potential energy profiles for rotation about the C_6-N_1 and $C_{18}-O_{17}$ bonds, corresponding roughly to the cuts in the potential energy map indicated in Fig. 2 by the horizontal and perpendicular broken lines.

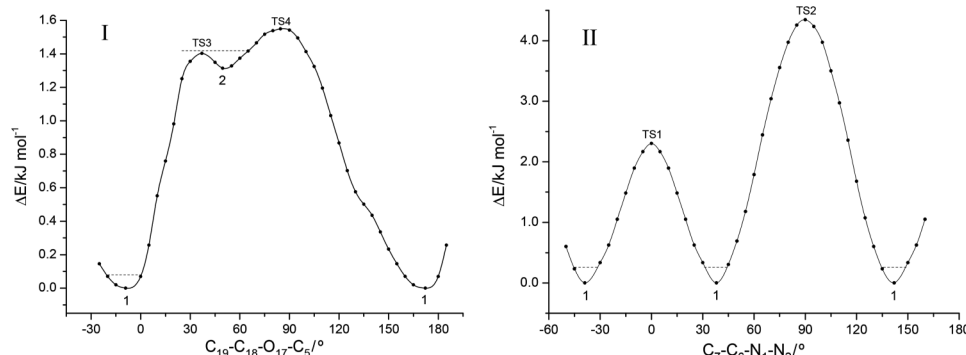
Fig. 2. B3LYP/6-311++G(d,p) potential energy map describing the change in the potential energy (zero-point uncorrected energy values) as a function of the C_6-N_1 and $C_{18}-O_{17}$ torsional coordinates. The map was built with the driving coordinates fixed at values differing by 20° and by optimizing all of the remaining coordinates. The positions of the minima are indicated.



The dihedral angle around the C_6-N_1 bond (A in Fig. 1) defines the relative orientation of the phenyl substituent and tetrazole rings. The calculations show that in the two minimum-energy structures, the planes of these two rings make an angle of approximately 30° (36° in form **1** and 32° in **2**). The value of the angle between the planes of these two rings is largely determined by the balance among three factors: (i) steric repulsions between the two substituents on the tetrazole ring (phenyl and phenoxy), which favor a nonplanar geometry, (ii) conjugation of the π -electron systems of both rings, favoring their coplanarity, and (iii) weak intramolecular hydrogen-bond-like interaction between the ortho-hydrogen atoms of the phenyl ring and the negatively charged O_{17} and N_2 atoms located at the tetrazole side of the molecule, with the $C_7-H_{12}\cdots N_2$ and $C_{11}-H_{16}\cdots O_{17}$ interactions being expected to favor noncoplanar and coplanar arrangements of the two rings, respectively. It is interesting to note that the $C_7-H_{12}\cdots N_2$ and $C_{11}H_{16}\cdots O_{17}$ H-bond distances are somewhat shorter in **2** than in **1** (259 and 247 pm, respectively, versus 263 and 254 pm), indicating that these two weak hydrogen-bond-type interactions in the higher energy minimum **2** are slightly stronger than in the more stable form **1**. The angle between the planes of the phenyl and tetrazole rings is smaller in form **2** than in form **1** and the orientation of the phenyl group of the phenoxy substituent relatively to the tetrazole ring is also different in the two forms. The approximate coplanarity of the tetrazole and phenoxy moieties in form **1** clearly imposes a stronger steric hindrance to the coplanarity of the phenyl substituent of the tetrazole ring compared with the more skewed arrangement of the tetrazole and phenoxy moieties present in form **2** (see Fig. 1).

In form **1**, the two transition states for rotation of the phenyl group (about C_6-N_1), one corresponding to the structure with coplanar tetrazole (TS1) and phenyl rings and the other to a geometry where these rings are perpendicular (TS2), have energies higher than the minimum energy structure of 2.30 and 4.35 kJ mol^{-1} , respectively (see Fig. 3, trace II). The higher energy of the transition state bearing the two rings perpendicular, compared with that where the two rings are coplanar, results from the lack of

Fig. 3. B3LYP/6-311++G(d,p) calculated potential energy profiles for internal rotation of the phenyl groups (trace I, belonging to the phenoxy substituent; trace II, directly connected to the tetrazole moiety). These potential energy profiles were calculated by incrementing the value of the scanned coordinate in steps of 5° and letting all other coordinates relax to their optimal values. In all geometries along the potential energy profile (I), the conformations about the C₆-N₁ and O₁₇-C₅ axes optimize to approximately 30° and 180°, respectively, while along the potential energy profile II, the conformations about the C₁₈-O₁₇ and O₁₇-C₅ axes both optimize to approximately 180°. Horizontal broken lines indicate the zero-point levels for the two minimum energy structures.



π -electron delocalization between the two rings in the first case. Nevertheless, it shall also be stressed that the conjugation between the phenyl and tetrazole rings is reduced. This can be concluded not only by taking into account the small energy difference between the energies of the two transition states TS1 and TS2 but also by considering the length of the C₆-N₁ bond (142.7 pm), which does not differ too much from a typical C-N single bond in alkylamines (within the 145–147 pm range),³⁴ and differs very much from a typical double bond (for instance, like that found in methylenimine, H₂C=NH: 127.3 pm).³⁵ In simple diazines (pyrazine, pyrimidine, and pyridazine), where the CN bond lengths have a bond order of approximately 1.5, conjugated system, the bond lengths are approximately 133.5 pm,^{36–38} i.e., also considerably shorter than the C₆-N₁ distance in 5PPT.

Internal rotation around the C₁₈-O₁₇ bond (C in Fig. 1) determines the relative orientation of the phenyl ring of the phenoxy substituent and the tetrazole ring. This internal rotation corresponds to the most flexible coordinate of the molecule and is essentially the one distinguishing the two minima. In the lowest energy form **1**, the two rings are nearly coplanar (the planes of the two rings make an angle smaller than 10°), which ensures both a more relevant π -electron delocalization and a favorable geometry for establishment of a stabilizing intramolecular hydrogen bond interaction (C-H₂₈···N₄; see Fig. 1). The hydrogen bond distance (H₂₈···N₄) is 225 pm, i.e., considerably shorter than the sum of the van der Waals radii of hydrogen and nitrogen atoms (~275 pm). On the other hand, in the higher energy structure **2**, this interaction does not exist, since the tetrazole ring and the phenyl ring of the phenoxy substituent are significantly deviated from coplanarity (the angle between the planes of the two rings is ~80°). Considering that the C-H₂₈···N₄ intramolecular hydrogen bond is the main interaction distinctive of the two forms, one can roughly estimate the strength of such an interaction in form **1** as being of the order of magnitude of the energy difference between the two forms, i.e., ~1–2 kJ mol⁻¹.

The potential energy profile for rotation about the C₁₈-O₁₇ bond, shown in Fig. 3 (trace I), reveals that the energy barriers separating the higher energy minimum **2** from the most stable form **1** are very low, amounting only to 0.09 and 0.24 kJ mol⁻¹ (TS3 and TS4, respectively). The calculated (scaled) frequency of the torsion around the C₁₈-O₁₇ bond for form **2** is 16.8 cm⁻¹, which yields a zero-point energy for this mode at the minimum (0.10 kJ mol⁻¹), which surpasses the energy barrier of 0.09 kJ mol⁻¹ taken from the bottom of the potential well. This means that form **2** does not in fact correspond to a stable structure, since upon taking into account the zero-point energy correction, one can

Table 1. B3LYP/6-311++G(d,p)-calculated bond lengths (pm) and angles (°) around the central ether linkage in tetrazole ethers 5MPP,³⁹ 5EPT⁴⁰, and 5PPT.

Molecule	Structural parameter			
	O-C _t	C _a -O	C-O-C	C _a -O-C-N(ph)
5MPT	132.4	144.7	115.4	177.0
5EPT	132.3	146.0	115.7	176.6
5PPT	132.7	140.4	125.2	178.1

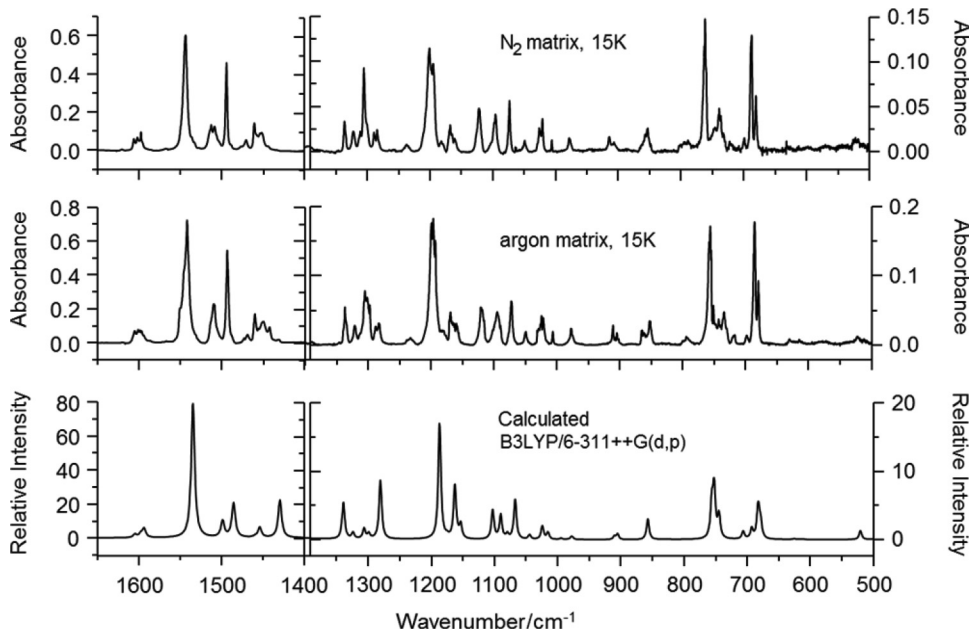
Note: Subscripts “t” and “a” designate the tetrazole and aryl/alkyl substituents, respectively.

conclude that it relaxes barrierlessly to **1**. In practical terms, this result shows that 5PPT has actually only one conformer in the gas phase (form **1**), which one can expect to be also the sole species present in the low-temperature matrices investigated in this study (see below).

The calculated bond lengths and angles around the central ether linkage in 5PPT are compared with corresponding data previously obtained by our groups for 5-methoxy-1-phenyltetrazole (5MPT)³⁹ and 5-ethoxy-1-phenyltetrazole (5EPT)⁴⁰ (Table 1). In all of these compounds, the tetrazole ring and the heavy atom skeleton of the second ether substituent are preferentially oriented in a near coplanar fashion, with the latter pointing in the opposite direction relatively to the phenyl substituent of the tetrazole (C_a-O-C-N(Ph)). These data are in keeping with results obtained from crystallographic analysis of a library of aryloxy- and naphthoxytetrazoles.²² As mentioned in the Introduction section, due to the electron-withdrawing nature of the tetrazole ring, for all ethers the central ether linkage is much shorter on the tetrazole ether side (O-C_t around 132 pm) than on the aryl or alkyl side (C_a-O ranging from 140 to 146 pm). The constancy of the O-C_t bond length in the three compounds demonstrates that the extent of electron delocalization associated with the tetrazole ring and the ether oxygen atom lone-electron pair is not significantly influenced by the nature of the second ether substituent (either it being alkyl or aryl). On the other hand, the C_a-O bond is considerably shorter in 5PPT than in the two alkyl ethers, as could be expected considering that the carbon atom is hybridized sp² and also the likely existing electron delocalization involving the aryl fragment and the oxygen atom lone-electron pairs.

C-O-C bond angles range from 115° in the alkoxytetrazoles to 125° in phenoxytetrazole. The larger angle observed in phenoxytetrazole results from both the more relevant steric hindrance between the tetrazole and phenyl moiety of the phenoxy sub-

Fig. 4. Comparison of the infrared spectra of monomeric 5PPT isolated in argon and nitrogen matrices (15 K) with the B3LYP/6-311++G(d,p)-calculated spectrum of the compound. The calculated spectrum was simulated using Lorentzian functions with a full-width-at-half-maximum of 5 cm⁻¹ with frequencies scaled by 0.978.



stituent and the higher sp²-type hybridization character exhibited by the ether oxygen atom in this compound.

Infrared spectra of matrix-isolated 5PPT

The infrared spectra of the matrix-isolated 5PPT in argon and nitrogen matrices are presented in Fig. 4 together with the B3LYP/6-311++G(d,p)-predicted spectrum of the compound (form 1). The experimental spectra exhibit considerable site-splitting (especially in case of the most intense bands associated with more polar molecular fragments, which can be expected to be more sensitive to the local environment), revealing that the 5PPT molecules occupy multiple matrix sites, in both the argon and nitrogen matrices. Annealing experiments showed that the different local environments shall have very similar stability, since the observed band components resulting from site-splitting do not experience intensity changes upon temperature variation, i.e., no site conversions could be induced in an efficient way within the range of temperatures investigated (15–25 K).

As can be seen in Fig. 4, despite the splitting observed in the bands of the experimental spectra, the agreement between these spectra and the calculated one is very good, enabling a full, reliable assignment of the experimental bands. The assignments are provided in Table 2 (see supporting information Table S1 for definition of coordinates).

Belonging to the C₁ symmetry point group, the 5PPT molecule has 78 fundamental vibrations, all of them expected to be active in the infrared. In agreement with the spectral data previously obtained for 5MPT and 5EPT,^{39,40} the IR spectrum of 5PPT may be considered as formed by three groups of bands associated respectively with the vibrational modes of the phenyl group, tetrazolyl ring, and phenoxy substituent. The bands comprised in the first group appear in the spectrum of 5PPT at nearly the same frequencies observed for 5MPT³⁹ and 5EPT.⁴⁰ This result indicates that the nature of the substituent in position 5 of the tetrazole ring has a minor influence on the internal potential of the phenyl group linked to position 1. Such a finding is in consonance with the conclusions extracted above based on structural and energetic data for the three compounds.

In contrast with the vibrations belonging to the phenyl substituent, the tetrazole ring vibrations are, as one could anticipate,

substantially affected by the nature of the substituent at position 1, and some differ considerably among the three compounds. Among the most intense bands in the IR spectra of 5PPT associated with modes originated mainly in this group ($\nu(\text{N}=\text{C})$, $\nu(\text{N}=\text{N})$, $\nu(\text{N}-\text{N}')$, $\nu(\text{C}-\text{N})$, $\nu(\text{N}-\text{N})$, and $\delta(\text{T-ring } 2)$), the two CN stretching modes appear to be the most sensitive to the nature of the substituent connected to position 1 of the tetrazole ring. For example, the $\nu(\text{N}=\text{C})$ vibration appears as a doublet at 1299/1298 cm⁻¹ in 5EPT and⁴⁰ at 1572/1571 cm⁻¹ in 5MPT³⁹ and as a multiplet centered at approximately 1450 cm⁻¹ in 5PPT (see Table 2).

The effects of the nature of the substituent on the C–O stretching vibrations closely follow the trends extracted from the structural data discussed above: the $\nu(\text{C}_\text{ring}-\text{O})$ frequency is similar in the three compounds (1567/1565/1553 cm⁻¹ in 5EPT,⁴⁰ 1489 cm⁻¹ in 5MPT,³⁹ and 1551/1545/1542/1532 cm⁻¹ in 5PPT), while the frequency of the $\nu(\text{O}-\text{C}_\text{a})$ (subscript “a” standing for aryl or alkyl) vibration is much higher in the case of 5PPT (1200/1198/1193 cm⁻¹), where the O–C_a bond is much shorter, than in 5MPT (746 cm⁻¹)³⁹ and 5EPT (903/901/900/886/885 cm⁻¹).⁴⁰

UV-laser-induced photochemistry of matrix-isolated 5PPT

It has been shown^{17,18,41,42} that the preferred reaction occurring upon subjecting tetrazoles to UV irradiation corresponds to molecular nitrogen extrusion, with formation of several different isomeric species, which include the diazirine, nitrilimine, cyanamide, and carbodiimide (Scheme 2). In general, nitrilimine and diazirine species are short lived under photolysis conditions because they quickly convert into the photostable isomeric carbodiimide or, less frequently, cyanamide.^{41,42}

Upon UV laser irradiation ($\lambda = 250 \text{ nm}$) (see supporting information Fig. S2 the UV absorbance spectrum of 5PPT) of the monomer of 5PPT isolated in argon, the infrared spectrum of the compound lost intensity, while new bands developed, indicating that the compound underwent a photochemical transformation. Figure 5 presents the difference spectrum obtained by subtracting the spectrum of the deposited matrix from that recorded after 70 min of UV irradiation. In the figure, a theoretical difference spectrum is also plotted, where the bands pointing down correspond to the reactant (5PPT) and those pointing up to N-phenoxy-N'-phenylcarbodiimide. Among the possible photoproducts, this

Table 2. Proposed assignments for the IR spectra of 5PPT isolated in argon and nitrogen matrices, B3LYP/6-311++G(d,p)-calculated spectrum for the compound (form 1), and results of normal coordinate analysis.

Description	Observed		Calculated		
	Argon matrix	Nitrogen matrix	Frequency	IR intensity	Potential energy distribution
$\nu(\text{C}-\text{H})_{\text{b}} 1$	3119/3116/3115	3122/3119	3166.4	15.3	$S_{26}(99)$
$\nu(\text{C}-\text{H})_{\text{a}} 2'$	3107	3105	3143.4	1.1	$S_{16}(54) + S_{17}(38)$
$\nu(\text{C}-\text{H})_{\text{a}} 1$	3087/3084	3087	3140.7	0.5	$S_{15}(90)$
$\nu(\text{C}-\text{H})_{\text{b}} 2'$	3080	3084	3129.0	3.9	$S_{27}(63) + S_{29}(24)$
$\nu(\text{C}-\text{H})_{\text{a}} 2'$	3075/3078	3078	3123.6	14.7	$S_{17}(41) + S_{18}(39) + S_{16}(15)$
$\nu(\text{C}-\text{H})_{\text{b}} 2''$	3055	3054	3121.0	17.3	$S_{28}(75) + S_{29}(19)$
$\nu(\text{C}-\text{H})_{\text{a}} 3''$	3043/3044	3043	3112.8	9.1	$S_{19}(94)$
$\nu(\text{C}-\text{H})_{\text{b}} 3''$			3109.9	9.6	$S_{30}(89)$
$\nu(\text{C}-\text{H})_{\text{a}} 3'$	3030/3027/3025	3031/3027	3102.6	0.0	$S_{18}(52) + S_{16}(31) + S_{17}(16)$
$\nu(\text{C}-\text{H})_{\text{b}} 3'$			3100.7	0.1	$S_{29}(57) + S_{27}(33) + S_{28}(10)$
$\nu(\text{Ph}_b\text{-ring} 4)$	1605	1606	1606.9	0.3	$S_{23}(35) + S_{21}(27)$
$\nu(\text{Ph}_a\text{-ring} 2)$	1601	1602	1604.4	15.1	$S_{10}(62) + S_{47}(19)$
$\nu(\text{Ph}_a\text{-ring} 4)$	1599/1597/1595	1597	1597.5	16.0	$S_{12}(63) + S_{46}(10)$
$\nu(\text{Ph}_b\text{-ring} 2)$			1593.5	41.3	$S_{21}(26) + S_{23}(30) + S_{52}(11)$
$\nu(\text{C}-\text{O})$	1551sh/1545/1542/1532sh	1544	1534.6	623.1	$S_7(38) + S_3(34)$
$\delta(\text{C}-\text{H})_{\text{a}} 2$	1513sh/1510/1509	1513sh/1512/1509/1502sh	1498.9	75.9	$S_{45}(49) + S_{13}(29) + S_6(10)$
$\delta(\text{C}-\text{H})_{\text{b}} 2$	1494	1494	1485.7	160.2	$S_{50}(61) + S_{24}(32)$
$\delta(\text{C}-\text{H})_{\text{b}} 3$	1474	1470	1459.9	4.8	$S_{25}(27) + S_{51}(26)$
$\delta(\text{C}-\text{H})_{\text{a}} 3$	1469		1454.2	47.4	$S_{14}(30) + S_{46}(26) + S_{44}(10)$
$\nu(\text{N}=\text{C})$	1460/1456/1451/1444/1442/1431	1460/1455/1451/1450/1442/1430sh	1429.9	174.7	$S_4(31) + S_6(12) + S_3(10)$
$\nu(\text{N}=\text{N})$	1339sh/1336/1334sh	1338sh/1337/1334	1339.6	41.9	$S_1(63) + S_{44}(20)$
$\delta(\text{C}-\text{H})_{\text{a}} 1$	1321	1323	1324.8	2.4	$S_{44}(53) + S_{11}(15)$
$\delta(\text{C}-\text{H})_{\text{b}} 1$			1324.2	4.6	$S_{49}(62) + S_{22}(13)$
$\nu(\text{Ph}_b\text{-ring} 3)$	1297	1290	1306.8	11.8	$S_{22}(61) + S_{49}(16)$
$\nu(\text{Ph}_a\text{-ring} 3)$	1288/1285/1283/1282	1284	1299.5	5.8	$S_{11}(69) + S_1(14) + S_{44}(10)$
$\delta(\text{T-ring} 1)$	1305/1303/1301	1311/1305/1300sh	1281.1	67.6	$S_3(22) + S_6(18) + S_{22}(15) + S_{36}(11)$
$\nu(\text{O}-\text{C})$	1200/1198/1193	1201/1195	1187.4	133.0	$S_{52}(28) + S_8(25) + S_{21}(13)$
$\delta(\text{C}-\text{H})_{\text{a}} 4$	1179	1182	1175.5	2.4	$S_{47}(76) + S_{10}(24)$
$\delta(\text{C}-\text{H})_{\text{b}} 4$	1171/1169/1167/1164/1162	1168/1165	1163.2	61.2	$S_{52}(31) + S_{53}(19) + S_8(14)$
$\delta(\text{C}-\text{H})_{\text{a}} 5$	1160/1159	1161	1159.0	1.3	$S_{48}(65) + S_{11}(13) + S_{46}(12)$
$\delta(\text{C}-\text{H})_{\text{b}} 5$			1154.0	16.1	$S_{53}(48) + S_{52}(16) + S_{51}(10) + S_{22}(10)$
$\nu(\text{N}-\text{N}'')$	1121/1120/1118/1116	1121	1103.3	33.7	$S_5(24) + S_2(15) + S_{14}(11) + S_{46}(11)$
$\delta(\text{T-ring} 2)$	1100/1098/1095/1094/1089	1097/1096	1090.6	27.8	$S_{37}(35) + S_2(31) + S_{14}(10)$
$\nu(\text{Ph}_b\text{-ring} 6)$			1080.1	5.6	$S_{25}(48) + S_{51}(34) + S_{53}(10)$
$\nu(\text{Ph}_a\text{-ring} 6)$	1072/1071	1073	1067.7	45.8	$S_{14}(30) + S_{37}(25) + S_{46}(14) + S_5(11)$
$\nu(\text{Ph}_a\text{-ring} 5)$	1049	1049	1044.9	5.2	$S_{13}(40) + S_{45}(21) + S_{51}(12)$
$\nu(\text{Ph}_b\text{-ring} 5)$	1029/1028/1026	1029sh/1026	1024.6	15.4	$S_{24}(50) + S_{50}(23) + S_{20}(15)$
$\nu(\text{Ph}_a\text{-ring} 1)$	1021	1021	1015.7	7.8	$S_9(29) + S_{38}(29) + S_{13}(17)$
$\delta(\text{Ph}_a\text{-ring} 1)$	1007	1006	995.6	0.1	$S_{38}(49) + S_9(48)$
$\delta(\text{Ph}_b\text{-ring} 1)$			994.8	1.4	$S_{41}(62) + S_{20}(33)$
$\gamma(\text{C}-\text{H})_{\text{a}} 4$			983.5	0.1	$S_{56}(25) + S_{71}(25) + S_{70}(22) + S_{72}(14)$
$\nu(\text{C}-\text{N})$	978/977	978/976	978.6	2.9	$S_2(26) + S_{37}(19) + S_4(11) + S_{77}(10)$
$\nu(\text{N}-\text{N})$			976.7	1.4	$S_{77}(21) + S_{59}(17) + S_2(11)$
$\gamma(\text{C}-\text{H})_{\text{a}} 2$	960	n.o.	964.8	0.1	$S_{58}(27) + S_{72}(25) + S_{70}(18) + S_{69}(15)$ + $S_{73}(14)$
$\gamma(\text{C}-\text{H})_{\text{b}} 1$		n.o.	960.8	0.2	$S_{75}(33) + S_{61}(24) + S_{74}(13) + S_{78}(12)$
$\gamma(\text{C}-\text{H})_{\text{a}} 1$	912sh/910	914/909	910.6	3.7	$S_{73}(29) + S_{69}(28) + S_{71}(25) + S_{57}(11)$
$\gamma(\text{C}-\text{H})_{\text{b}} 5$	907/905/902	907/905sh	905.5	6.4	$S_{78}(29) + S_{76}(25) + S_{74}(24) + S_{60}(13)$
$\nu(\text{Ph}_b\text{-ring} 1)$	866/864/863/862/860/859/ 855sh/853/851/850sh	863/860/858/854/853/852sh/848	857.5	24.0	$S_{36}(21) + S_{20}(20) + S_8(13) + S_{41}(12)$
$\gamma(\text{C}-\text{H})_{\text{a}} 4$	795	801/794/788	828.6	0.1	$S_{73}(29) + S_{69}(27) + S_{70}(23) + S_{72}(20)$
$\gamma(\text{C}-\text{H})_{\text{b}} 4$			824.9	0.2	$S_{74}(35) + S_{76}(26) + S_{77}(20) + S_{75}(17)$
$\gamma(\text{C}-\text{H})_{\text{a}} 3$	759	762	756.2	38.4	$S_{71}(33) + S_{66}(21) + S_{72}(10)$
$\gamma(\text{C}-\text{O})$	756/755/752	761/759sh	752.4	57.1	$S_{76}(22) + S_{68}(13)$
$\gamma(\text{C}-\text{H})_{\text{b}} 3$	743/734/730sh	745/739/737/732	744.7	26.3	$S_{76}(35)$
$\tau(\text{T-ring} 1)$	719/717	722	706.3	8.9	$S_{55}(45) + S_{65}(31) + S_{54}(20)$
$\tau(\text{Ph}_a\text{-ring} 1)$	699	699	692.8	11.6	$S_{54}(43) + S_{56}(26)$
$\gamma(\text{C}-\text{H})_{\text{b}} 2$	687sh/686/685	689/688/687	683.3	10.6	$S_{59}(34) + S_{75}(12) + S_{77}(10)$
$\tau(\text{Ph}_b\text{-ring} 1)$			682.2	29.3	$S_{56}(16) + S_{59}(16) + S_{54}(14)$
$\delta(\text{Ph}_a\text{-ring} 3)$	680/679sh	682sh/680/679sh	678.6	17.0	$S_{40}(36) + S_{64}(12) + S_{36}(11)$
$\delta(\text{Ph}_b\text{-ring} 3)$	630	n.o.	625.5	0.9	$S_{43}(39) + S_{32}(14)$
$\delta(\text{Ph}_a\text{-ring} 2)$	614	n.o.	615.2	0.3	$S_{39}(83)$
$\delta(\text{Ph}_b\text{-ring} 2)$		n.o.	611.2	0.4	$S_{42}(86)$

Table 2 (concluded).

Description	Observed		Calculated		
	Argon matrix	Nitrogen matrix	Frequency	IR intensity	Potential energy distribution
$\gamma(\text{C}-\text{N})$	524	521	520.4	10.2	$S_{67}(31) + S_{57}(13) + S_{33}(12) + S_{43}(10)$
$\tau(\text{Ph}_b\text{-ring} 2)$	493	490	492.6	7.1	$S_{68}(57) + S_{60}(20) + S_{76}(57)$

Note: Wavenumbers (scaled by 0.978) in cm^{-1} , calculated intensities in km mol^{-1} . ν , bond stretching; δ , bending; γ , rocking; τ , torsion; $\text{Ph}_a\text{-ring}$, phenyl ring; $\text{Ph}_b\text{-ring}$, phenyl ring of the phenoxy substituent; T-ring, tetrazole ring; n.o., not observed; sh, shoulder. Calculated data for spectral region not experimentally investigated (description: frequency (cm^{-1}) (IR intensity (km mol^{-1}); potential energy distribution: $\gamma(\text{N}-\text{N}): 458.6 [3.9] S_{34}(22) + S_{33}(11) + S_{43}(11)$, $\tau(\text{Ph}_b\text{-ring} 3): 411.7 [0.0] S_{61}(70)$, $\tau(\text{Ph}_a\text{-ring} 3): 407.5 [0.2] S_{58}(71)$, $\nu(\text{N}-\text{C}): 369.3 [1.8] S_{40}(19) + S_{35}(18) + S_6(17)$, $\tau(\text{T-ring} 2): 343.6 [1.5] S_{45}(22) + S_{57}(17) + S_{55}(10)$, $\delta(\text{Ph}_b\text{-O}): 305.5 [4.0] S_{35}(24) + S_{36}(11) + S_7(10)$, $\delta(\text{Ph}_a\text{-N}): 277.8 [0.9] S_{55}(25) + S_{65}(22) + S_{34}(16)$, $\tau(\text{Ph}_a\text{-ring} 2): 223.3 [0.7] S_{60}(28) + S_{57}(10)$, $\delta(\text{O-C-N}): 211.9 [0.1] S_{60}(23) + S_{57}(15) + S_{32}(10)$, $\delta(\text{C-O-Ph}_b): 155.6 [2.5] S_{31}(36) + S_{35}(16) + S_{33}(12) + S_{34}(10)$, $\gamma(\text{C}-\text{N}): 103.3 [0.8] S_{65}(65)$, $\delta(\text{C-N}): 63.9 [0.8] S_{33}(26) + S_{32}(15) + S_{31}(12)$, $\tau(\text{Ph}_a\text{-N}): 43.3 [0.8] S_{63}(65) + S_{62}(15)$, $\tau(\text{C-O}): 29.1 [0.0] S_{62}(51) + S_{64}(39) + S_{63}(16)$, $\tau(\text{Ph}_b\text{-O}): 12.9 [0.5] S_{64}(65) + S_{62}(28)$.

Scheme 2. Possible photoproducts of tetrazole ring N₂ photoelimination. **1**, carbodiimide; **2**, cyanamide; **3**, diazirine; **4**, nitrilimine (propargylic (**4a**) and allenic (**4b**) forms).

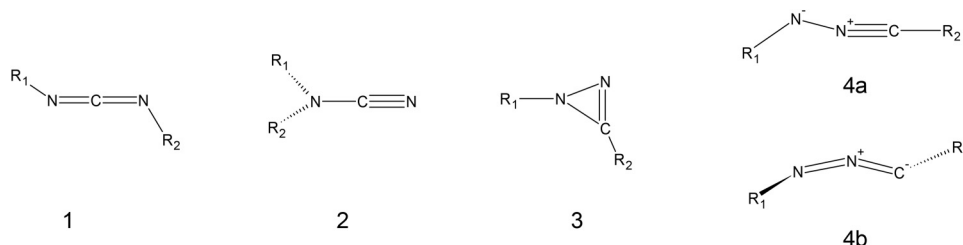


Fig. 5. (A) Calculated difference infrared spectrum (carbodiimide minus 5PPT) and (B) experimental difference spectrum (UV-irradiated argon matrix, $\lambda = 250 \text{ nm}$, 70 min minus deposited matrix). See text for an explanation of the observed smearing of intensity of experimental bands of the carbodiimide at approximately 1200 and 885 cm^{-1} .

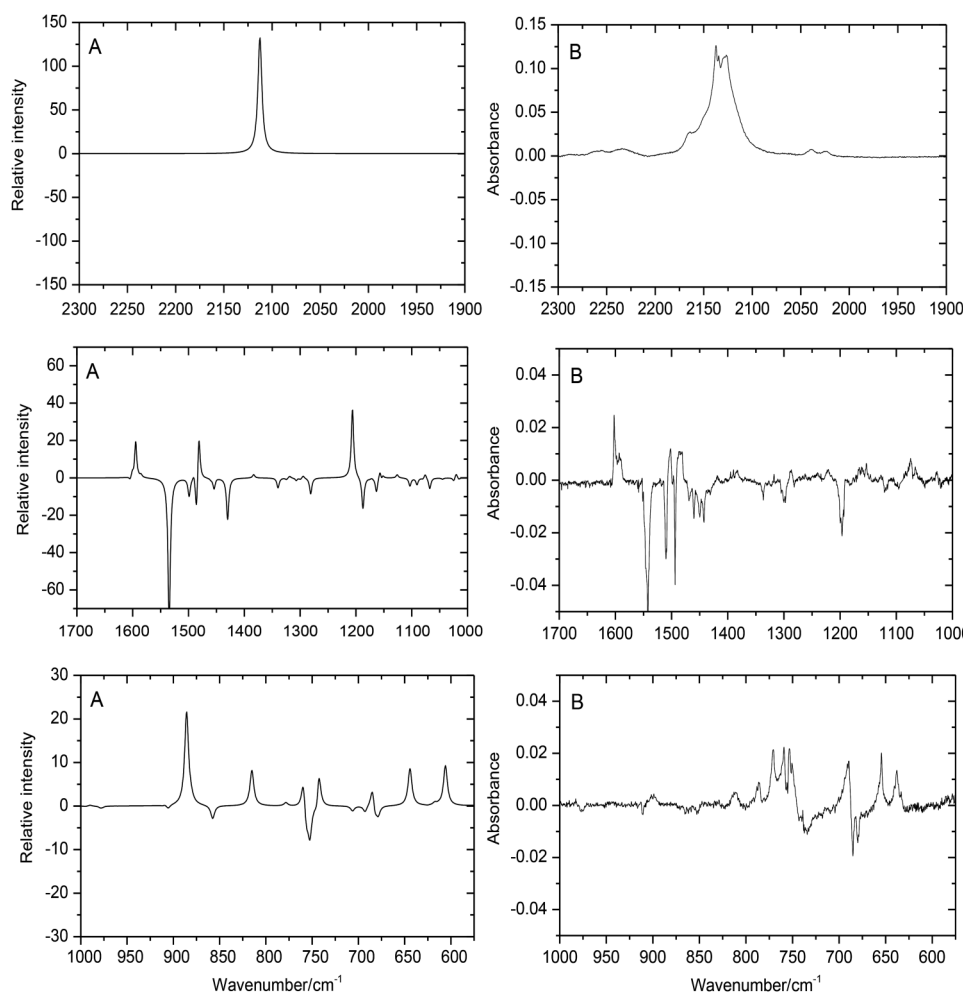


Table 3. Proposed assignments for the carbodiimide photoproduct and calculated (B3LYP/6-311++G(d,p))-calculated IR spectrum for this molecule.

Approximate description	Calculated			Approximate description	Calculated		
	ν	IR intensity	Observed ν		ν	IR intensity	Observed ν
ν CH	3152.8	1.8	3098	γ CH	979.5	0.0	n.o.
	3129.7	6.6			962.9	0.1	n.o.
	3125.5	9.0			962.5	0.2	n.o.
	3121.8	14.1	3074		950.2	0.0	n.o.
	3118.2	22.0			909.9	4.4	n.o.
	3112.9	9.9			885.7	168.8	902/899
	3104.9	2.2	3053		880.9	7.2	
	3104.4	12.0			826.6	0.3	812
	3097.5	1.6	3036		815.1	64.1	
	3096.5	1.7			812.4	0.0	
ν NCN as.	2112.6	1040.9	2286/2257/2236/2164/2149/2138/2135/2130/2128/2127/2118/2040/2024	δ CNO, δ CCC	778.4	5.9	785
ν CC	1600.6	19.0	1602/1600/1597/1594/1590	γ CH	759.6	51.4	771/761
	1598.0	1.1			742.7	68.4	753/751
	1594.5	192.3			684.9	32.6	691
	1585.0	10.3			683.2	23.7	
δ CH	1490.4	29.4	1502/1489/1486/1481	τ ring	644.2	67.4	655
	1481.3	195.4			617.4	4.2	638/634
	1454.6	2.5	n.o.		613.1	1.4	
	1449.7	2.9	n.o.		606.0	72.3	
ν NCN s.	1383.2	14.4	1395/1390/1383	δ CCC	560.8	31.2	583/578
	1321.9	0.9	1318		515.7	11.0	n.i.
δ CH	1318.6	8.1		τ ring	498.5	9.8	
	1305.0	1.6	1288		465.2	0.8	
	1294.6	10.5			410.9	0.0	
	1206.2	289.6	1262/1249/1241/1222/1216		409.8	0.1	
ν CC	1171.9	3.0	n.o.	δ CCN	403.6	0.7	
	1157.0	31.3	1166/1161		348.1	19.1	
	1156.6	2.7			288.0	0.3	
	1151.9	13.6	1153/1146		221.1	0.0	
ν C–N	1126.1	13.5	1127	δ Skeletal	203.2	4.8	
	1076.1	11.0	1074		158.5	0.9	
δ CH	1075.5	7.7	1056	γ CN	99.7	4.1	
	1021.4	2.4	1027		74.3	0.6	
	1020.3	17.5			31.8	0.3	
	995.1	0.7	n.o.		18.4	0.3	
δ CCC	989.9	1.8	n.o.	τ Ph–N	13.6	0.4	

Note: Calculated frequencies (ν (cm $^{-1}$)) scaled by 0.978; IR intensities in km mol $^{-1}$. ν , bond stretching; δ , bending; γ , rocking; τ , torsion; Ph, phenyl ring; as., antisymmetric; s., symmetric; n.o., not observed; n.i. not investigated.

is the one whose characteristic spectrum better matches the spectrum of the photoproduced species. The comparison of the calculated infrared spectra of the other putative photoproducts (specifically, the isomeric nitrilimine, diazirine, and cyanamide; see Scheme 2 and Fig. S3) with that of the observed photoproduct allowed us to safely discard them as contributors to the observed spectrum.

A strong indication supporting the identification of the carbodiimide as the observed product of photolysis of 5PPT is the presence in the spectrum of the characteristic intense and structured band centered at \sim 2133 cm $^{-1}$, exhibiting satellite bands centered at \sim 2250 and \sim 2230 cm $^{-1}$ (see Fig. 5; top panels), which is a very characteristic spectroscopic signature of carbodiimides (ν N=C=N antisymmetric stretching).^{41–44} In the studied low-frequency region between 1650 and \sim 600 cm $^{-1}$, the predicted spectrum for the carbodiimide fits also rather well the experimental spectrum of the photoproduct (see Table 3 for proposed assignments), with two notable exceptions: the calculations predict the ν C–O and ν N–O stretching modes of the molecule to appear as relatively intense bands at approximately 1206 and 886 cm $^{-1}$, respectively, while no prominent bands are observed at these frequencies in the experimental spectrum. However, a broad band spreading from 893 to 905 cm $^{-1}$ is indeed observed in the experimental spectrum, which can be correlated with the ν N–O vibration of the

carbodiimide, while in the 1215–1265 cm $^{-1}$ range, the experimental spectrum presents a series of at least five low-intensity bands that one can assign to the ν C–O vibration. The main reason for the observed intensity smearing of the ν C–O and ν N–O bands shall be ascribed to the fact that these two vibrations are very much sensitive to the molecular conformation about the N–O bond of the molecule. The τ N–O torsional coordinate is in fact extremely flexible, the calculated vibrational frequency for this mode being only 13.5 cm $^{-1}$. This result correlates with a very flat τ N–O torsional potential, leading to large amplitude torsional movements even if one restricts the movement to the zero vibrational level, and also to a rather slow vibration compared with the ν C–O and ν N–O stretching modes. This band intensity smearing phenomenon has been observed in other molecules exhibiting low frequency, large amplitude torsional vibrations, e.g., azobenzene,⁴⁵ and dimethyloxalate.⁴⁶ For the considered carbodiimide, calculations of the vibrational frequencies along the τ N–O torsion,⁴⁷ for values of the torsional angle deviated from the equilibrium geometry within \pm 60°, showing that in the studied spectral region, only three vibrations with large enough predicted IR intensity (above 5 km mol $^{-1}$) have frequencies that are significantly influenced by the torsional angle. These are precisely the ν C–O and ν N–O modes plus the ν N=C=N antisymmetric stretching (which, as mentioned above, is a broad band and does also exhibit quite pronounced satellite

bands, in line with the present interpretation). For these three modes, the calculated frequency shifts are 20, 30, and 27 cm⁻¹, respectively, which are considerably larger than the mean absolute shift for all of the remaining 52 modes lying in the probed spectral region, which is smaller than 5 cm⁻¹.

It is also interesting to note that the carbodiimide is, among the isomeric molecules shown in Scheme 2, the species having the lowest energy. According to the performed B3LYP/6-311++G(d,p) calculations on all of those molecules, the carbodiimide is 1.69, 54.13, and 55.02 kJ mol⁻¹ more stable than its isomeric cyanamide, nitrilimine, and diazirine, respectively. This is an additional argument in favor of the observation of the carbodiimide as the final product of photolysis of 5PPT.

Conclusions

5-Phenoxy-1-phenyltetrazole was isolated in argon and N₂ cryogenic matrices and its molecular structure, conformational landscape, vibrational signature, and photochemistry were investigated by infrared spectroscopy and theoretical calculations (DFT(B3LYP)/6-311++G(d,p)). Two different minima were located on the potential energy surface of the molecule, both being eightfold degenerate by symmetry and belonging to the C₁ symmetry point group. However, consideration of zero-point vibrational energy allowed concluding that the higher energy minimum shall relax barrierlessly to the lower energy form so that in the gas phase, the compound exists in a single conformer. These theoretical predictions were confirmed by the experimental results, with only one conformer of 5PPT contributing to the infrared spectra of the compound isolated in argon and N₂ matrices. Structural details of the different conformations and intramolecular interactions operating in 5PPT were used to understand the conformational preferences of the compound.

The infrared spectra of 5PPT in the studied matrices were fully assigned and interpreted with help of normal coordinate analysis.

UV laser irradiation ($\lambda = 250$ nm) of matrix-isolated 5PPT was found to lead to photocleavage of the compound to the corresponding carbodiimide accompanied by N₂ release. Relevant characteristics of the experimental spectrum of the observed photoproduct, specifically the intensity smearing noticed in the ν N—O and ν C—O spectral regions, were interpreted based on the effect of the low-frequency, large-amplitude τ N—O mode in this compound.

Supplementary material

Supplementary material is available with the article through the journal Web site at <http://nrcresearchpress.com/doi/suppl/10.1139/cjc-2015-0025>. Supporting information: Figure S1 with the ¹H NMR spectrum of 5PPT in CDCl₃, Fig. S2 with the UV-visible spectra of 5PPT in ethanol, Fig. S3 with calculated infrared spectra for considered possible products resulting from photoelimination of N₂ from 5PPT, and Table S1 with the definition of the internal coordinates used in the normal modes analysis calculations performed on 5PPT.

Acknowledgements

The authors gratefully acknowledge Fundação para a Ciência e a Tecnologia (FCT), Portugal (Projects PEst-OE/QUI/UI0313/2014 and PEst-C/MAR/LA0015/2014, cofunded by QREN-COMPETE-UE), and CCMAR for financial support. A.B. and L.C. acknowledge FCT and CCMAR, respectively, for the award of a postdoctoral grant (reference SFRH/BPD/66154/2009) and a research fellowship.

References

- Bugalho, S. C. S.; Maçãs, E. M. S.; Cristiano, M. L. S.; Fausto, R. *Phys. Chem. Chem. Phys.* **2001**, *3*, 3541. doi:[10.1039/b103344c](https://doi.org/10.1039/b103344c).
- Mohite, P.-B.; Bhaskar, V. H. *Int. J. PharmTech Res.* **2011**, *3*, 1557.
- Sandmann, G.; Schneider, C.; Boger, P. Z. *Naturforsch. C* **1996**, *51*, 534.
- Zhao-Xu, C.; Heming, X. *Int. J. Quantum Chem.* **2000**, *79*, 350. doi:[10.1002/1097-461X\(2000\)79:6<350::AID-QUA3>3.3.CO;2-K](https://doi.org/10.1002/1097-461X(2000)79:6<350::AID-QUA3>3.3.CO;2-K).
- Koldobskii, G. I.; Ostrovskii, V. A.; Poplavskii, V. S. *Khim. Geterot. Soed.* **1981**, *10*, 1299.
- Gaponik, P. N.; Voitekhovich, S. V.; Ivashkevich, O. A. *Russ. Chem. Rev.* **2006**, *75*, 507. doi:[10.1070/RCC2006v07n06ABEH003601](https://doi.org/10.1070/RCC2006v07n06ABEH003601).
- Stierstorfer, J.; Tarantik, K. R.; Klapötke T. M. *Chem. Eur. J.* **2009**, *15*, 5775. doi:[10.1002/chem.200802203](https://doi.org/10.1002/chem.200802203).
- Herr, R. J. *Bioorg. Med. Chem.* **2002**, *10*, 3379. doi:[10.1016/S0968-0896\(02\)00239-0](https://doi.org/10.1016/S0968-0896(02)00239-0).
- May, B. C. H.; Abell, A. D. *J. Chem. Soc., Perkin Trans. 1* **2002**, *172*. doi:[10.1039/B109128j](https://doi.org/10.1039/B109128j).
- Bugalho, S. C. S.; Lapinski, L.; Cristiano, M. L. S.; Frija, L. M. T.; Fausto, R. *Vib. Spectrosc.* **2002**, *30*, 213. doi:[10.1016/S0924-2031\(02\)00028-0](https://doi.org/10.1016/S0924-2031(02)00028-0).
- Hussey, B. J.; Johnstone, R. A. W.; Entwistle, J. D. *Tetrahedron* **1982**, *38*, 3775. doi:[10.1016/0040-4020\(82\)80091-4](https://doi.org/10.1016/0040-4020(82)80091-4).
- Johnstone, R. A. W.; Wilby, A. H.; Entwistle, I. D. *Chem. Rev.* **1985**, *85*, 129. doi:[10.1021/cr00066a003](https://doi.org/10.1021/cr00066a003).
- Cristiano, M. L. S.; Johnstone, R. A. W.; Price, P. J. *J. Chem. Soc. Perkin Trans. 1* **1996**, *1453*. doi:[10.1039/P19960001453](https://doi.org/10.1039/P19960001453).
- Araújo, N. C. P.; Brigas, A. F.; Cristiano, M. L. S.; Frija, L. M. T.; Guimarães, E. M. O.; Loureiro, R. M. S. J. *Mol. Catal. A* **2004**, *215*, 113. doi:[10.1016/j.molcata.2003.12.033](https://doi.org/10.1016/j.molcata.2003.12.033).
- Frija, L. M. T.; Cristiano, M. L. S.; Guimarães, E. M. O.; Martins, N. C.; Loureiro, R. M. S. S.; Bickley, J. F. *J. Mol. Catal. A* **2005**, *242*, 241. doi:[10.1016/j.molcata.2005.08.022](https://doi.org/10.1016/j.molcata.2005.08.022).
- Gómez-Zavaglia, A.; Reva, I. D.; Frija, L. M. T.; Cristiano, M. L. S.; Fausto, R. *J. Photochem. Photobiol., A* **2006**, *179*, 243. doi:[10.1016/j.jphotochem.2005.08.021](https://doi.org/10.1016/j.jphotochem.2005.08.021).
- Frija, L. M. T.; Ismael, A.; Cristiano, M. L. S. *Molecules* **2010**, *15*, 3757. doi:[10.3390/molecules15053757](https://doi.org/10.3390/molecules15053757).
- Frija, L. M. T.; Cristiano, M. L. S.; Gómez-Zavaglia, A.; Reva, I.; Fausto, R. *J. Photochem. Photobiol., C* **2014**, *18*, 71. doi:[10.1016/j.jphotochemrev.2013.09.001](https://doi.org/10.1016/j.jphotochemrev.2013.09.001).
- Gómez-Zavaglia, A.; Reva, I. D.; Frija, L. M. T.; Cristiano, M. L. S.; Fausto, R. *J. Phys. Chem. A* **2005**, *109*, 7967. doi:[10.1021/jp0517706](https://doi.org/10.1021/jp0517706).
- Gómez-Zavaglia, A.; Reva, I.; Frija, L. M. T.; Cristiano, M. L. S.; Fausto, R. *J. Mol. Struct.* **2006**, *786*, 182. doi:[10.1016/j.molstruc.2005.08.019](https://doi.org/10.1016/j.molstruc.2005.08.019).
- Ismael, A.; Cristiano, M. L. S.; Fausto, R.; Gómez-Zavaglia, A. *J. Phys. Chem. A* **2010**, *114*, 13076. doi:[10.1021/jp109215q](https://doi.org/10.1021/jp109215q).
- Alves, J. A. C.; Barkley, J. V.; Brigas, A. F.; Johnstone, R. A. W. *J. Chem. Soc., Perkin Trans. 2* **1997**, *669*. doi:[10.1039/A607912A](https://doi.org/10.1039/A607912A).
- Frisch, M. J.; Trucks, G. W.; Schlegel, H. B.; Scuseria, G. E.; Robb, M. A.; Cheeseman, J. R.; Scalmani, G.; Barone, V.; Mennucci, B.; Petersson, G. A.; Nakatsuji, H.; Caricato, M.; Li, X.; Hratchian, H. P.; Izmaylov, A. F.; Bloino, J.; Zheng, G.; Sonnenberg, J. L.; Hada, M.; Ehara, M.; Toyota, K.; Fukuda, R.; Hasegawa, J.; Ishida, M.; Nakajima, T.; Honda, Y.; Kitao, O.; Nakai, H.; Vreven, T.; Montgomery, J. A., Jr.; Peralta, J. E.; Ogliaro, F.; Bearpark, M.; Heyd, J. J.; Brothers, E.; Kudin, K. N.; Staroverov, V. N.; Kobayashi, R.; Normand, J.; Ragahavachari, K.; Rendell, A.; Burant, J. C.; Iyengar, S. S.; Tomasi, J.; Cossi, M.; Rega, N.; Millam, M. J.; Klene, M.; Knox, J. E.; Cross, J. B.; Bakken, V.; Adamo, C.; Jaramillo, J.; Gomperts, R.; Stratmann, R. E.; Yazyev, O.; Austin, A. J.; Cammi, R.; Pomelli, C.; Ochterski, J. W.; Martin, R. L.; Morokuma, K.; Zakrzewski, V. G.; Voth, G. A.; Salvador, P.; Dannenberg, J. J.; Dapprich, S.; Daniels, A. D.; Farkas, Ö.; Foresman, J. B.; Ortiz, J. V.; Cioslowski, J.; Fox, D. J. *Gaussian 09*, Revision D.01; Gaussian, Inc.: Wallingford, CT, 2009.
- Becke, A. D. *Phys. Rev. A* **1988**, *38*, 3098. doi:[10.1103/PhysRevA.38.3098](https://doi.org/10.1103/PhysRevA.38.3098).
- Lee, C. T.; Yang, W. T.; Parr, R. G. *Phys. Rev. B* **1988**, *37*, 785. doi:[10.1103/PhysRevB.37.785](https://doi.org/10.1103/PhysRevB.37.785).
- Vosko, S. H.; Wilk, L.; Nusair, M. *Can. J. Phys.* **1980**, *58*, 1200. doi:[10.1139/p80-159](https://doi.org/10.1139/p80-159).
- Frisch, M. J.; Head-Gordon, M.; Pople, J. A. *Chem. Phys. Lett.* **1990**, *166*, 281. doi:[10.1016/0009-2614\(90\)80030-H](https://doi.org/10.1016/0009-2614(90)80030-H).
- Császár, P.; Pulay, P. *J. Mol. Struct.* **1984**, *114*, 31. doi:[10.1016/S0022-2860\(84\)87198-7](https://doi.org/10.1016/S0022-2860(84)87198-7).
- Peng, C.; Schlegel, H. B. *Isr. J. Chem.* **1994**, *33*, 449.
- Irikura, K. K. *Program SYNSPEC*; National Institute of Standards and Technology: Gaithersburg, MD.
- Kereszty, G.; Jaloszky, G. *J. Mol. Struct.* **1971**, *10*, 304. doi:[10.1016/0022-2860\(71\)87090-4](https://doi.org/10.1016/0022-2860(71)87090-4).
- Rostkowska, H.; Lapinski, L.; Nowak, M. *J. Vib. Spectrosc.* **2009**, *49*, 43. doi:[10.1016/j.vibspec.2008.04.012](https://doi.org/10.1016/j.vibspec.2008.04.012).
- Pulay, P.; Fogarasi, G.; Pang, F.; Boggs, J. E. *J. Am. Chem. Soc.* **1979**, *101*, 2550. doi:[10.1021/ja00504a009](https://doi.org/10.1021/ja00504a009).
- Batista de Carvalho, L. A. E.; Teixeira-Dias, J. J. C.; Fausto, R. *Struct. Chem.* **1990**, *1*, 533. doi:[10.1007/BF00674129](https://doi.org/10.1007/BF00674129).
- Pearson, R.; Lovas, F. *J. Chem. Phys.* **1977**, *66*, 4149. doi:[10.1063/1.434490](https://doi.org/10.1063/1.434490).
- Cradock, S.; Purves, C.; Rankin, D. W. H. *J. Mol. Struct.* **1990**, *220*, 193. doi:[10.1016/0022-2860\(90\)80109-W](https://doi.org/10.1016/0022-2860(90)80109-W).
- Fernholt, L.; Römming, C. *Acta Chem. Scand.* **1978**, *32*, 271. doi:[10.3891/acta.chem.scand.32a-0271](https://doi.org/10.3891/acta.chem.scand.32a-0271).
- Bormans, B. J. M.; de With, G.; Mijlhoff, F. C. *J. Mol. Struct.* **1977**, *42*, 121. doi:[10.1016/0022-2860\(77\)87035-X](https://doi.org/10.1016/0022-2860(77)87035-X).
- Gómez-Zavaglia, A.; Reva, I. D.; Frija, L. M. T.; Cristiano, M. L. S.; Fausto, R. *J. Photochem. Photobiol., A* **2006**, *180*, 175. doi:[10.1016/j.jphotochem.2005.10.012](https://doi.org/10.1016/j.jphotochem.2005.10.012).
- Frija, L. M. T.; Reva, I. D.; Gómez-Zavaglia, A.; Cristiano, M. L. S.; Fausto, R. *J. Phys. Chem. A* **2007**, *111*, 2879. doi:[10.1021/jp068556h](https://doi.org/10.1021/jp068556h).

- (41) Bégué, D.; Qiao, G. G.; Wentrup, C. *J. Am. Chem. Soc.* **2012**, *134*, 5339. doi:[10.1021/ja2118442](https://doi.org/10.1021/ja2118442).
- (42) Nunes, C. M.; Araújo-Andrade, C.; Fausto, R.; Reva, I. *J. Org. Chem.* **2014**, *79*, 3641. doi:[10.1021/jo402744f](https://doi.org/10.1021/jo402744f).
- (43) King, S. T.; Strope, J. H. *J. Chem. Phys.* **1971**, *54*, 1289. doi:[10.1063/1.1674967](https://doi.org/10.1063/1.1674967).
- (44) Pagacz-Kostreva, M.; Mucha, M.; Weselski, M.; Wierzejewska, M. *J. Photochem. Photobiol. A* **2013**, *251*, 118. doi:[10.1016/j.jphotochem.2012.10.023](https://doi.org/10.1016/j.jphotochem.2012.10.023).
- (45) Duarte, L.; Fausto, R.; Reva, I. *Phys. Chem. Chem. Phys.* **2014**, *16*, 16919. doi:[10.1039/C4CP00240G](https://doi.org/10.1039/C4CP00240G).
- (46) Lopes, S. B.; Lapinski, L.; Fausto, R. *Phys. Chem. Chem. Phys.* **2002**, *4*, 5952. doi:[10.1039/B206270B](https://doi.org/10.1039/B206270B).
- (47) The τ N-O mode does not mix with others, so that optimization of geometry of the molecule for different values of this coordinate leads to vanishing forces on atoms along all of the remaining coordinates, thus making meaningful the vibrational calculations for geometries other than the equilibrium geometry.